Transaction B: Mechanical Engineering
Vol. 16, No. 2, pp. 159–167

SCIENTIA IRANICA

Simulation of Turbulent Flow Through Porous Media Employing a v2f Model

R. Bahoosh Kazerooni[1] and S. Kazemzadeh Hannani[1,*]

Abstract. *In this article, a v2f model is employed to conduct a series of computations of incompressible flow in a periodic array of square cylinders simulating a porous media. A Galerkin/least-squares finite element formulation employing equal order velocity-pressure elements is used to discretize the governing equations. The Reynolds number is varied from 1000 to 84,000 and different values of porosities are considered in the calculations. Results are compared to the available data in the literature. The v2f model exhibits superior accuracy with respect to $k-\varepsilon$ results and is closer to LES calculations. The macroscopic pressure gradients for all porosities studied showed a good agreement with Forchheimer-extended Darcy's law in the range of large Reynolds numbers.*

Keywords: *Porous media; Turbulent flow; Volume averaging; v2f model.*

INTRODUCTION

Porous media can be found in a wide variety of engineering applications and natural systems. For the design of engineering systems, it is generally desirable to calculate the pressure drop across the porous medium and to predict the flow field characteristics. Most porous materials used in traditional engineering applications have very small pores and small permeability, therefore, the fluid speed is relatively small. In these porous materials, the dominant flow regime is the laminar flow. High speed fluid flow through porous media with considerable permeability can lead to turbulent flow within the pores.

Dybbs and Edwards [1] have studied experimentally the characteristics of turbulent flow through porous medium using laser anemometry and flow visualization techniques. They reported that four flow regimes may occur through porous media. Following [1], the first type of flow is the Darcy or creeping flow regime, when the flow is dominated by viscous forces and which occurs at $\mathrm{Re}_p < 1$ (based on the average particle dimension and the average pore velocity). At $\mathrm{Re}_p \sim O(1)$, boundary layers begin to develop near the solid boundaries of the pores. The inertial flow regime is the second type of flow, which is initiated at $\mathrm{Re}_p = 1 - 10$, when the boundary layers become more pronounced and an "inertial core" appears. The developing of the "core" flows outside the boundary layers is the reason for the non-linear relationship between the pressure drop and flow rate. As the Re_p increases, the "core" flows enlarge in size and their influence becomes more and more significant to the overall flow picture. This steady non-linear laminar flow regime persists up to $\mathrm{Re}_p \sim 150$. The third flow regime detected by [1] is an unsteady laminar flow field in the Reynolds number ranges of 150 to 300. At $\mathrm{Re}_p \sim 250$, the first evidence of unsteady flow is observed in the form of laminar wake oscillations in the pores. These oscillations take the form of traveling waves characterized by distinct periods, amplitudes and growth rates. In this flow regime, these oscillations exhibit preferred frequencies that seem to correspond to growth rates. Vortices form at $\mathrm{Re}_p \sim 250$ and persist up to $\mathrm{Re}_p \sim 300$. Finally, based on flow visualization techniques, a highly unsteady and chaotic flow regime, which occurs for $\mathrm{Re}_p > 300$ and which qualitatively resembles turbulent flow, is categorized as a fourth flow regime by [1].

Modeling turbulent flow through porous media is important in engineering applications, such as simulating compact heat exchangers, composite seawalls and composite break-waters, to mention just a few [2-5]. More traditional applications can be found in the

1. *Center of Excellence in Energy Conversion, Department of Mechanical Engineering, Sharif University of Technology, Tehran, P.O. Box 11155-9567, Iran.*
*. *Corresponding autor. E-mail: hannani@sharif.edu*

Received 5 March 2007; received in revised form 28 August 2007; accepted 23 September 2007

design of fluidized bed combustors and in enhancing petroleum extraction from reservoirs. Other practical phenomena of natural origin and environmental importance are the contaminants transported by air flow through forests and corps.

Masuoka and Takatsu [6] derived and solved a zero equation turbulence model for flow through porous media by use of the local volume-averaging technique. They modeled the effective eddy diffusivity as the algebraic sum of the eddy diffusivities estimated from two types of vortices: The pseudo vortex and the interstitial vortex. They studied turbulent flow and heat transfer through stacked spheres. Alvarez et al. [7] proposed and solved a one equation 'macroscopic' turbulence model. They derived a k equation, starting from a $k-l$ version of conventional RANS (Reynolds Averaged Navier-Stokes) models.

Two-equation 'macroscopic' turbulence models are also proposed in the literature. Antohe and Lage [8] derived a two-equation macroscopic turbulence model by applying the time averaging operator to the generalized model for flow through porous media (known as the Brinkman-Forchheimer-Extended Darcy model). Getachew et al. [9] extended Antohe's work by taking into account the Forchheimer term into higher order terms. Following another approach, Kuwahara et al. [10] and Nakayama and Kuwahara [11] proposed a two-equation macroscopic turbulence model obtained by spatially averaging the Reynolds-averaged Navier-Stokes equations and $k-\varepsilon$ model transport equations. For more information on 'macroscopic' modeling, see Pedras and Lemos [12] and the references cited by these authors.

Kuwahara et al. [10], Nakayama and Kuwahara [11] and Pedras and Lemos [12,13] conducted numerical experiments for turbulent flows through a periodic array of cylinders, using the conventional 'microscopic' two-equation turbulence model, based on RANS equations. Kuwahara et al. [14] performed the Large-Eddy Simulation (LES) to study the turbulent flow through porous media using a 'microscopic' point of view and compared the results with a two equation $k-\varepsilon$ model. Direct Numerical Simulations (DNS) are the best choice for validating the result of any turbulence model through porous media, which, however, will not be available for engineering applications in the near future, due to the large memory and CPU time requirements.

In this paper, to study turbulent flow through porous media, we have employed a v2f turbulence model using a 'microscopic approach'. The v2f model is a higher order turbulence model than conventional two-equation models. This model circumvents the use of wall functions and introduces a more realistic expression for eddy viscosity and predicts the impingement region more accurately (see below for details). During the last few years, the v2f (DNS based) turbulence model, originally introduced by Durbin [15], has become increasingly popular, due to its ability to correctly account for near-wall damping without the use of ad-hoc damping functions. Wall effects through porous media and the strong blockage of flow in the stagnation and impingement region of pores are very crucial, therefore, it seems that the v2f model is a good candidate.

Summarizing the introduction, turbulent flow is ubiquitous, occurring in macroscopic scales of the universe and galaxies, down to the interior of porous media. A turbulent simulation of porous media encounters two challenges. The first problem consists of presenting an accurate turbulence model mimicking the complex flow features in the pores. The second challenge is to develop a suitable 'macroscopic' turbulence model, substituting the complex topology of the pore structures, using the concept of space-time or time-space averaging (so-called black box model). The present work is focused on the first challenge.

GOVERNING EQUATIONS AND V2F MODEL

The flow is assumed incompressible. The mean flow variables satisfy the following Reynolds Averaged Navier-Stokes equations (RANS):

$$\nabla.\mathbf{U} = 0, \tag{1}$$

$$\frac{D\mathbf{U}}{Dt} = -\nabla p + \nabla.[(\nu+\nu_t)(\nabla\mathbf{U} + \nabla\mathbf{U}^T)]. \tag{2}$$

The v2f model is applied for evaluating ν_t. This is a general model that is valid up to the wall, circumventing the use of wall functions (see below).

The v2f model of Durbin [15-17] and Behnia et al. [18] consists of solving two additional equations, with respect to the standard k and ε model, the wall-normal stress, $\overline{v^2}$, transport equation and an elliptic relaxation function, f, equation. This model was developed for improving the modeling of wall effects and, more precisely, uses the contribution of wall normal stress to obtain the eddy viscosity. The Boussinesq approximation is used for the stress-strain relationship as follows:

$$\overline{u_i u_j} - \frac{2}{3}\delta_{ij}k = -\nu_t\left(\frac{\partial U_i}{\partial x_j} + \frac{\partial U_j}{\partial x_i}\right). \tag{3}$$

The turbulent time scale, T, in Durbin's v2f model is [18]:

$$T = \min\left[\max\left[\frac{k}{\varepsilon}, C_T\sqrt{\frac{\nu}{\varepsilon}}\right], \frac{0.6k}{2\sqrt{3}C_\mu\overline{v^2}S}\right]. \tag{4}$$

The strain-rate magnitude, S, in Equation 4 is defined as:

$$S = \sqrt{S_{ij} S_{ij}}. \tag{5}$$

ν is the kinematics viscosity, S_{ij} is the strain rate tensor, and the turbulent length scale, L, is [18]:

$$L = C_L \max\left[\min\left[\frac{k^{3/2}}{\varepsilon}, \frac{k^{3/2}}{\sqrt{3}C_\mu \overline{v^2} S}\right], C_\eta \frac{\nu^{3/4}}{\varepsilon^{1/4}}\right]. \tag{6}$$

C_μ, C_L, C_T and C_η, which are model constants, will be defined in Equations 20.

The Durbin's v2f model can be summarized by the following four transport equations:

$$\frac{\partial k}{\partial t} + U_j \frac{\partial k}{\partial x_j} = \frac{\partial}{\partial x_j}\left[\left(\nu + \frac{\nu_t}{\sigma_k}\right)\frac{\partial k}{\partial x_j}\right] + P_k - \varepsilon, \tag{7}$$

$$\frac{\partial \varepsilon}{\partial t} + U_j \frac{\partial \varepsilon}{\partial x_j} = \frac{\partial}{\partial x_j}\left[\left(\nu + \frac{\nu_t}{\sigma_k}\right)\frac{\partial \varepsilon}{\partial x_j}\right] + \frac{C_{\varepsilon 1} P_k - C_{\varepsilon 2}}{T}, \tag{8}$$

$$\frac{\partial \overline{v^2}}{\partial t} + U_j \frac{\partial \overline{v^2}}{\partial x_j} = \frac{\partial}{\partial x_j}\left[\left(\nu + \frac{\nu_t}{\sigma_k}\right)\frac{\partial \overline{v^2}}{\partial x_j}\right] - \overline{v^2}\frac{\varepsilon}{k} + kf, \tag{9}$$

$$f - L^2 \nabla^2 f = (C_1 - 1)\frac{2/3 - \overline{v^2}/k}{T} + C_2 \frac{P_k}{k}. \tag{10}$$

P_k is the production of turbulent kinetic energy and is defined below (see Equation 19).

The term kf in Equation 9 represents the redistribution of turbulence energy from the streamwise component. This term is non-locally obtained by solving an elliptic relaxation equation for f [18].

The eddy viscosity, v_t, is given by:

$$v_t = C_\mu \overline{v^2} T. \tag{11}$$

The no slip boundary conditions, $(y \to 0)$, are approximated as:

$$k_w = 0, \qquad \varepsilon_w = \lim_{y \to 0} \frac{2\nu k}{y^2}, \tag{12a}$$

$$\overline{v_w^2} = 0, \qquad f_w = -20\overline{v^2} \lim_{y \to 0}\left[\frac{\overline{v^2}}{\varepsilon_w y^4}\right]. \tag{12b}$$

Variable y denotes the coordinate normal to the wall.

Lien & Kalitzin [19] proposed a modification of the v2f model that allows a simple explicit boundary condition at walls for elliptic relaxation. They introduced a new variable for f. This new variable is called compensated $\tilde{f}$ and is defined by:

$$\tilde{f} = f - 5\frac{\varepsilon \overline{v^2}}{k^2}. \tag{13}$$

With compensated $\tilde{f}$, Equation 10 is converted into:

$$\tilde{f} = L^2 \nabla^2 \tilde{f} = \left[\frac{2}{3}C_1 + (5 - C_1)\overline{v^2}/k\right]\frac{1}{T} + C_2 \frac{P_k}{k}. \tag{14}$$

According to this modification, the dissipation rate of Equation 9 is changed into:

$$\frac{\partial \overline{v^2}}{\partial t} + U_j \frac{\partial \overline{v^2}}{\partial x_j} = \frac{\partial}{\partial x_j}\left[\left(\nu + \frac{\nu_t}{\sigma_k}\right)\frac{\partial \overline{v^2}}{\partial x_j}\right] - 6\frac{\overline{v^2}}{T} + k\tilde{f}. \tag{15}$$

Using this modification, the upper limit of the realizability condition for stagnation flow is altered for the v2f model (for more details see [19]).

The modified turbulent time scale, T, is written as [19]:

$$T = \min\left[\max\left[\frac{k}{\varepsilon}, C_T\sqrt{\frac{\nu}{\varepsilon}}\right], \frac{0.6k}{\sqrt{6}C_\mu \overline{v^2} S}\right], \tag{16}$$

and the modified turbulent length, L, scale is [19]:

$$L = C_L \max\left[\min\left[\frac{k^{3/2}}{\varepsilon}, \frac{k^{3/2}}{\sqrt{6}C_\mu \overline{v^2} S}\right], C_\eta \frac{\nu^{3/4}}{\varepsilon^{1/4}}\right]. \tag{17}$$

S_{ij} is the mean strain rate tensor:

$$S_{ij} = (\partial U_i/\partial x_j + \partial U_j/\partial x_i)/2. \tag{18}$$

P_k, in Equations 7, 8 and 10, is the production of the turbulent kinetic energy and defined as:

$$P_k = \overline{u_i u_j}\partial U_i/\partial x_j. \tag{19}$$

The coefficients of the modified model are as follows [19]:

$$C_\mu = 0.22, \qquad C_L = 0.23, \qquad C_\eta = 85,$$

$$C_T = 6., \qquad C_1 = 0.4, \qquad C_2 = 0.3,$$

$$C_{\varepsilon 2} = 1.9, \qquad \sigma_k = 1., \qquad \sigma_\varepsilon = 1.3,$$

$$C_{\varepsilon 1} = 1.4\left[1 + 0.045\sqrt{\frac{k}{\overline{v^2}}}\right]. \tag{20}$$

It is known that the v2f model has a poor numerical stability. Sveningsson and Davidson [20] and Davidson et al. [21] proposed a simple modification for improving stability. The source term, $k\tilde{f}$, in the $\overline{v^2}$ transport (Equation 15), includes the modeled pressure strain term, which is damped near walls as compensated $\tilde{f}$ goes to zero. Since $\overline{v^2}$ represents the wall-normal stress, it should be the smallest normal stress, i.e. $\overline{v^2} \leq \overline{u^2}$ and $\overline{v^2} \leq \overline{w^2}$ and, thus, $\overline{v^2}$ should be smaller than $2k/3$ [20,21]. In the homogeneous region far away from

the wall, the Laplace term is assumed to be negligible i.e. $\frac{\partial^2 \tilde{f}}{\partial x_j \partial x_j} \to 0$, then Equation 14 reduces to:

$$\tilde{f} = \left[\frac{2}{3}C_1 + (5 - C_1)\overline{v^2}/k\right]\frac{1}{T} + C_2\frac{P_k}{k}. \quad (21)$$

On the region far away from the wall, the Laplace term is not negligible and, as a consequence, $\overline{v^2}$ gets too large, so that $\overline{v^2} \geq 2k/3$.

A modification is to use the right-hand side of Equation 14 as an upper bound on the source term, $k\tilde{f}$, in the $\overline{v^2}$-equation, i.e.:

The Source Term of the $\overline{v^2}$ transport equation =

$$\min\left\{k\tilde{f}, \left[\frac{2}{3}C_1 k + (5 - C_1)\overline{v^2}\right]\frac{1}{T} + C_2 P_k\right\}. \quad (22)$$

This modification ensures that $\overline{v^2} \leq 2k/3$ (for more details see [20,21]).

PROBLEM DEFINITION

The problem considered is shown schematically in Figure 1. In this figure a periodic array of square cylinders is shown. Based on the geometrical periodicity, only one structural unit is chosen for the computational domain. The selected area is shown in Figure 2. Therefore, the flow was solved only through the domain that is shown in Figure 2. By this technique, eddies larger than the scale of the porous structure are intentionally neglected, since such large eddies cannot be detected through a simulated porous medium.

The Reynolds number, $\mathrm{Re}_H = u_D H/\nu$, is based on the center-to-center distance, H. The porosity of this domain is calculated from $\phi = 1 - (D/H)^2$. The porosities used in the calculation of the present study

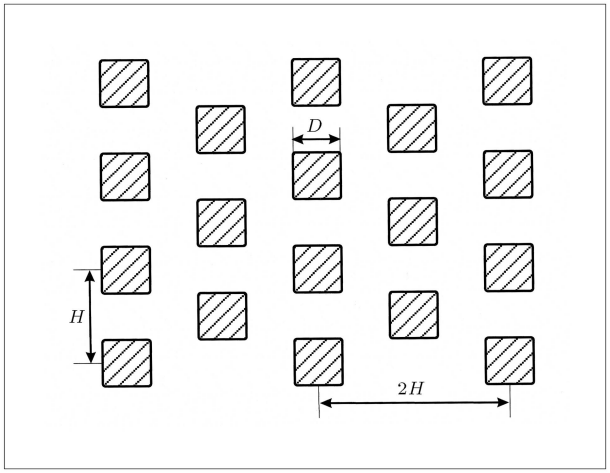

Figure 1. Periodic array of square cylinders.

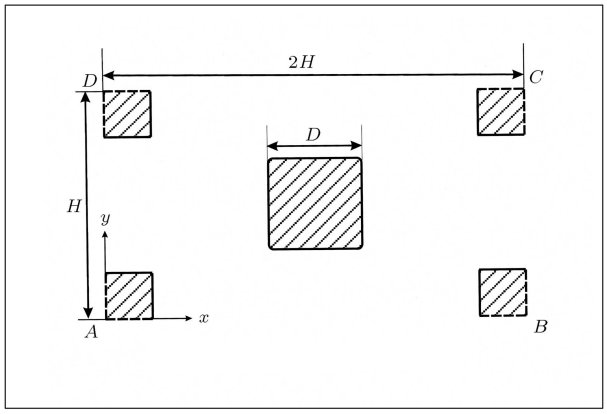

Figure 2. Structural unit chosen for the computation domain.

are selected as: $\phi = 0.3$, 0.4, 0.5, 0.64, 0.75, 0.84 and 0.95.

The boundary conditions related to periodicity are as follows:

$$\mathbf{U}(x = 0., y) = \mathbf{U}(x = 2H, y), \quad (23)$$

$$\mathbf{U}(x, y = 0) = \mathbf{U}(x, y = H). \quad (24)$$

The pressure gradient, p, in a periodically fully developed flow, can be expressed by [22]:

$$\frac{\partial p}{\partial x}(x, y) = -\beta + \frac{\partial P}{\partial x}(x, y), \quad (25)$$

where β is a constant and represents the overall pressure drop over the gradient imposed on the flow [22]. The function, $P(x, y)$, behaves in a periodic manner, so that:

$$P(x, y) = P(x + 2H, y + H). \quad (26)$$

The flow rate through the periodic cell (Figure 2) was set equal to unity by normalizing the variables and tuning the value of β.

The boundary conditions for turbulent kinetic energy and its dissipation are as follows:

$$k(x = 0., y) = k(x = 2H, y),$$

$$k(x, y = 0.) = k(x, y = H), \quad (27)$$

$$\varepsilon(x = 0., y) = \varepsilon(x = 2H, y),$$

$$k(x, y = 0.) = k(x, y = H). \quad (28)$$

The boundary conditions for Reynolds stress $\overline{v^2}$ and elliptic relaxation can be written as:

$$\overline{v^2}(x = 0., y) = \overline{v^2}(x = 2H, y),$$

$$\overline{v^2}(x, y = 0.) = \overline{v^2}(x, y = H), \quad (29)$$

$$\tilde{f}(x = 0., y) = \tilde{f}(x = 2H, y),$$

$$\tilde{f}(x, y = 0.) = \tilde{f}(x, y = H). \quad (30)$$

Boundary conditions for no slip boundaries were mentioned previously by Equations 12a and 12b.

RESULTS

The governing equations are numerically solved inside the domain and the results are shown in Figures 3 to 13.

The governing equations are discretized using a GLS (Galerkin/Least-Squares) finite element method, employing equal order interpolation for the velocity and pressure in conjunction with a pressure stabilizing method (see for more details [23,24]).

The Reynolds number, $\mathrm{Re}_H = u_D H/\nu$, is varied from 1000 to 500000. $u_D = \phi\langle U\rangle^f$ is a Darcian velocity and H is set equal to unity. In this work, the value of D is varied as 0.2236, 0.4, 0.5, 0.6, 0.7072, 0.7746 and 0.83667. The respected porosities are 0.95, 0.84, 0.75, 0.64, 0.5, 0.4 and 0.3. The Reynolds number based on H is converted to a Reynolds number based on D ($\mathrm{Re}_D = \mathrm{Re}_H \times D$) for comparing the present computations with the recent results of the literature [14]. D is the particle dimension and, in this study, Re_D is varied between 1000 to 84000.

For checking mesh-independency, the flow through the porosity of 0.84 has been solved at Re_H = 1000, 5000, 10000, 50000 and 100000 using 7508, 11948 and 17928 elements. The microscopic turbulent kinetic energy normalized by the square of Darcian velocity, k/u_D^2, of these solutions are shown at $x/H = 1$. The Reynolds number of Figure 3 is Re_D = 40000. The mesh stretching near the wall in these three solutions is similar. There is a good agreement between the solution data of 11948 and 17928 elements, therefore, mesh systems of the order of 12000 seem to be sufficiently accurate and all calculations presented below are obtained using this mesh system.

Regarding numerical convergence, the normalized residuals for all variables were brought down to 10^{-5}. For Reynolds numbers lower than 5×10^4, the under relaxation coefficient of U and p is 0.8, k and ε is 0.6, $\overline{v^2}$ and $\tilde{f}$ is 0.5 and, for Reynolds numbers equal to or greater than 5×10^4, the under relaxation coefficient of **U** and p is 0.7, k and ε is 0.4, $\overline{v^2}$ and $\tilde{f}$ is 0.3.

In Figure 4, streamlines are shown at Re_D = 40000 and for porosity = 0.84. Pressure contour solutions at Re_D = 40000 and porosity = 0.84 are shown in Figure 5. In Figure 6, turbulent kinetic energy contours are depicted at Re_D = 40000 for porosity = 0.84, employing the v2f model. The turbulent kinetic energy results are converted into macroscopic turbulent kinetic energy by applying the following volume average operator:

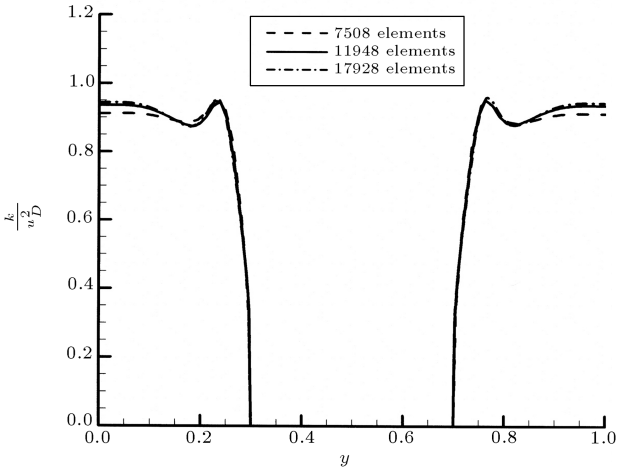

Figure 3. Normalized microscopic turbulent kinetic energy at Re_D = 40000 and $x/H = 1$.

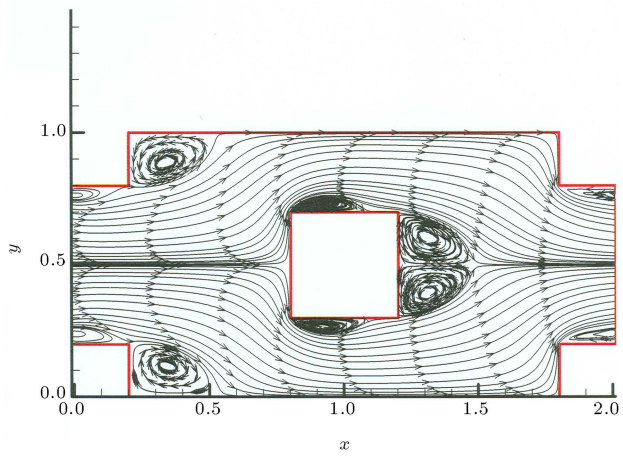

Figure 4. Streamlines for porosity = 0.84 and Re_D = 40000.

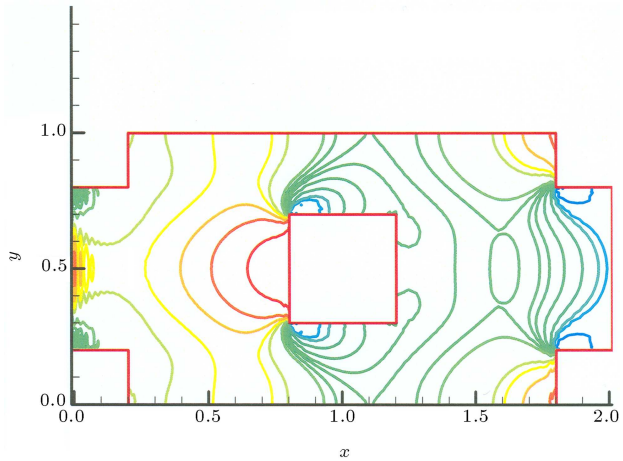

Figure 5. Pressure contours for porosity = 0.84 and Re_D = 40000.

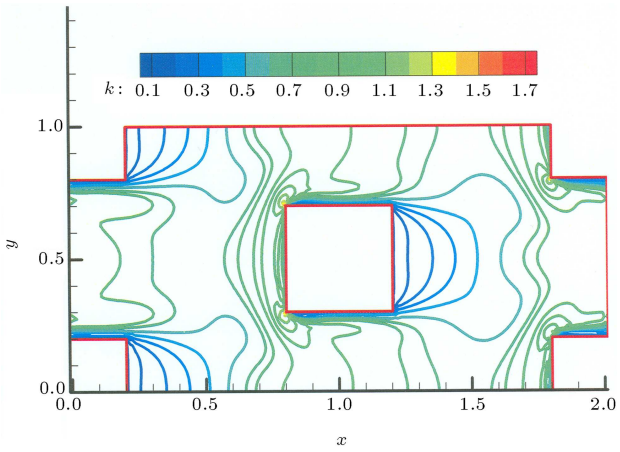

Figure 6. Normalized turbulent kinetic energy contours for porosity = 0.84 and $\mathrm{Re}_D = 40000$.

$$\langle k \rangle^f = \frac{1}{V_f} \int k dV, \tag{31}$$

$$V_f = \phi V. \tag{32}$$

The macroscopic turbulent kinetic data are normalized by the square of Darcian velocity, $\langle k \rangle^f / u_D^2$. These data are shown versus Reynolds number based on D, in Figures 7 to 10. These curves are sketched for various porosities of 0.84, 0.64, 0.5 and 0.3. The results of present calculations employing the v2f model have been compared with the results of [14] obtained using LES. The normalized macroscopic turbulent kinetic energy remained almost constant at large Reynolds numbers. It seems that the v2f model and LES both predict a Reynolds number independent normalized solution of k for large Re_D number flows. For the range of $\mathrm{Re}_D < 1000$, no logical correlation can be concluded between LES and v2f results. It is well known that turbulence model constants exhibit appreciable non-

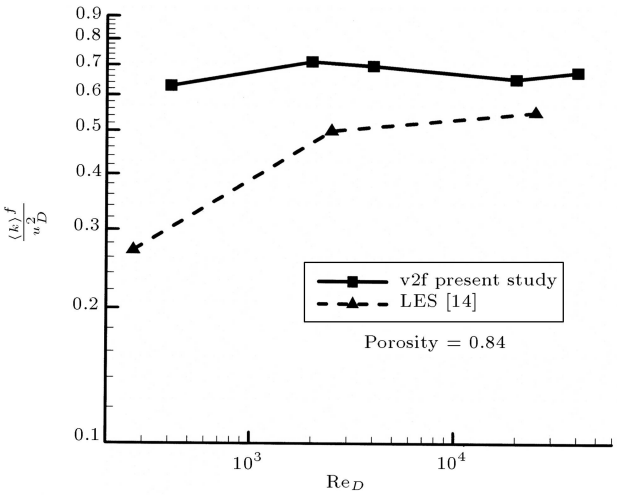

Figure 7. Normalized turbulent kinetic energy for porosity = 0.84.

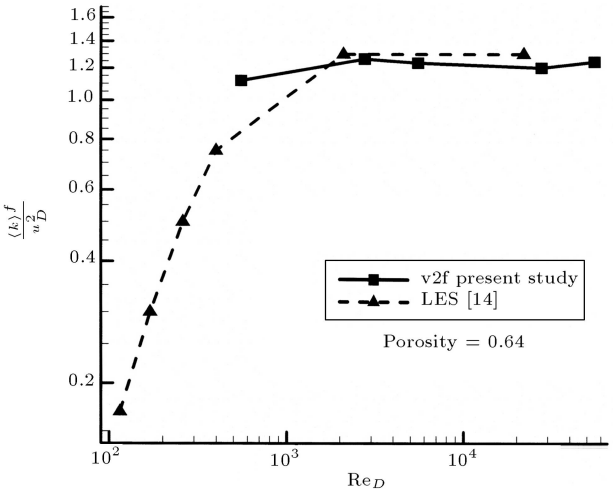

Figure 8. Normalized turbulent kinetic energy for porosity = 0.64.

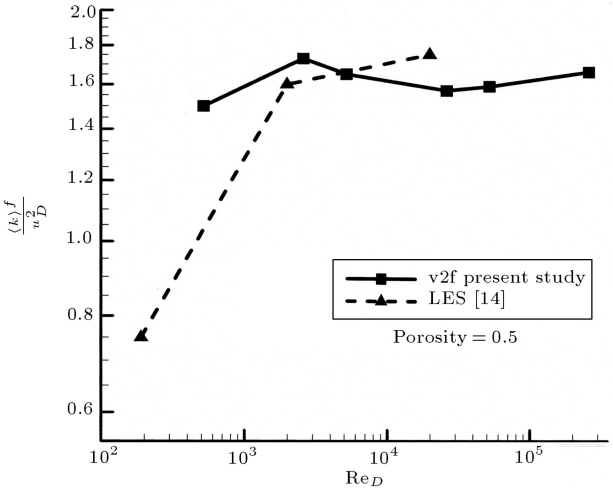

Figure 9. Normalized turbulent kinetic energy for porosity = 0.5.

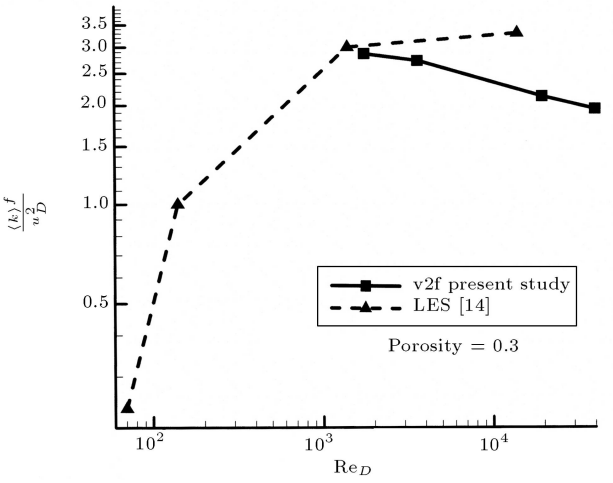

Figure 10. Normalized turbulent kinetic energy for porosity = 0.3.

universalities in the 'very low Reynolds number' limits ($\mathrm{Re}_D \sim 1000$) (see also [24,25]). We conjecture that for 'very low Reynolds number' turbulent flows, neither the present v2f model nor LES calculations of [14], which use an RNG $k-\varepsilon$ near wall model, are suitable for prediction with acceptable accuracy.

Macroscopic turbulent kinetic energies of all porosities in this study are depicted in Figure 11. The results of the present study are compared with the result of the LES solution of [14]. The slope of the present study data is smaller than the slope of LES and low Reynolds $k-\varepsilon$ model data. At lower porosities, the normalized macroscopic turbulent kinetic energy of LES [14] is larger than the v2f predictions. The difference can be attributed to the use of a renormalized group (RNG) subgrid scale model in LES [14], leading to overestimation of turbulent kinetic energy near stagnation or impingement regions. Figure 12 presents the normalized dissipation rate of turbulent kinetic energy for all porosities used in the present study. The present data are compared with the data of Nakayama and Kuwahara [11]. The dissipation rate of the turbulent kinetic energy of the present study is in good agreement with the results of [11].

The Forchheimer equation is known as a popular equation for estimating the pressure drop through porous media. Ergun's empirical equation, accounting for the Forchheimer drag in packed beds of particle diameter D, is given by [14]:

$$-\frac{d\langle p\rangle^f}{dx}\left[\frac{D}{\rho u_D^2}\right]=\frac{150(1-\phi)^2}{\phi}\left(\frac{\nu}{u_D D}\right)+1.75\frac{1-\phi}{\phi^3}. \tag{33}$$

Following Kuwahara et al. [14], the first term on the right hand side of Equation 33 could be neglected at high Reynolds number, therefore, Equation 33 is

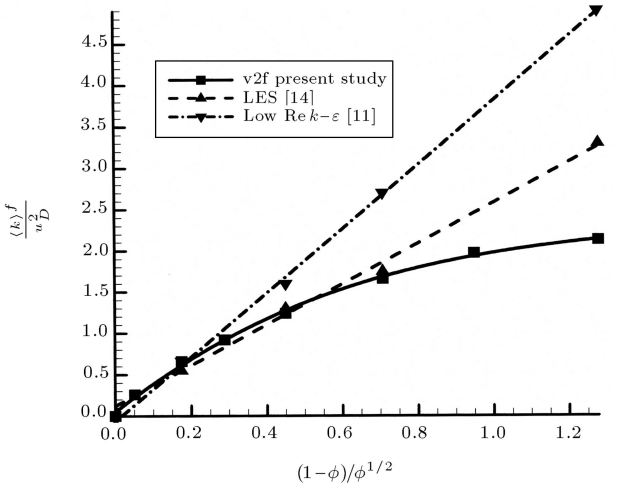

Figure 11. Normalized turbulent kinetic energy versus $(1-\phi)/\phi^{1/2}$.

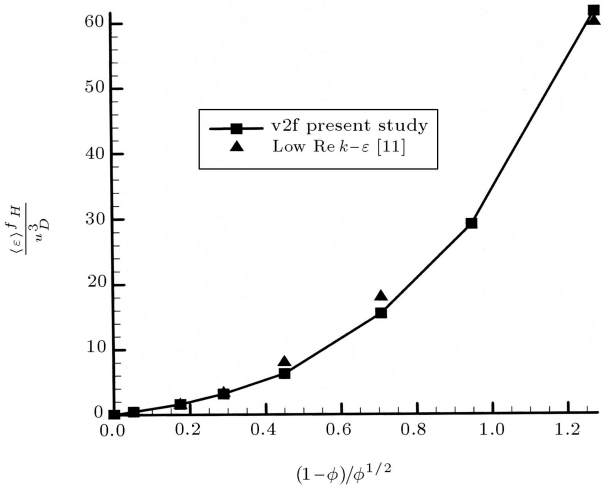

Figure 12. Normalized Dissipation rate of turbulent kinetic energy versus $(1-\phi)/\phi^{1/2}$.

simplified into Equation 34.

$$-\frac{d\langle p\rangle^f}{dx}\left[\frac{D}{\rho u_D^2}\right]=1.75\frac{1-\phi}{\phi^3}, \qquad (\mathrm{Re}_D>3000). \tag{34}$$

The dimensionless pressure gradient, $-d\langle p\rangle^f/dx\,[D/\rho u_D^2]$, is depicted in Figure 13. The line in this figure indicates the relation given by Equation 34. The pressure results of the present study are in good agreement with Forchheimer-extended Darcy's law.

CONCLUSION

A series of computations of incompressible flow in a periodic array of square cylinders simulating a porous media for various Reynolds numbers and different porosities, employing the v2f turbulence model, are carried out. The macroscopic turbulent kinetic energies

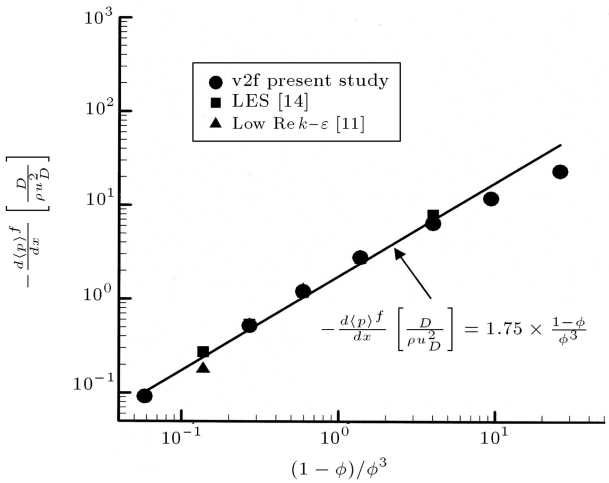

Figure 13. Dimensionless macroscopic pressure gradient versus $(1-\phi)/\phi^3$.

of this study are compared to the results available in the literature. Good agreement for Reynolds number is observed between LES and the present calculations. However, for a low Reynolds number flow of the order 1000, discrepancies between the results are noted. Further study is needed to elucidate the main shortcoming of simulations, both in the context of LES and turbulence modeling. The dissipation rate of the turbulent kinetic of the present study showed good agreement with the available results in the literature. The macroscopic pressure gradient results for all porosities are in concordance with the Forchheimer law. Our next step is to derive a 'macroscopic' v2f model for porous media. The v2f model could predict a better correlation for turbulent kinetic energy that is important for driving a macroscopic model for flow through porous media. It can be argued that in the macroscopic models, the inherent advantages of using a v2f model are not obvious and should be proved mathematically. However, various applications can be stated where porous and non-porous media calculations must be performed simultaneously. Indeed, the implementation of a single more accurate model would be very useful in these cases. The derivation, computation and validation of the macroscopic model will be conducted subsequently.

NOMENCLATURE

$C_\mu, C_L, C_\eta, C_2, C_{\varepsilon 1}$, $C_{\varepsilon 2}, C_T, \sigma_k, \sigma_\varepsilon$	turbulence model constants
D	particle diameter
f	elliptic relaxation function
$\tilde{f}$	compensated elliptic relaxation function
H	distance of two particles from each other
k	turbulent kinetic energy
$\langle k \rangle^f$	intrinsic volume average of turbulent kinetic energy
L	turbulent length scale
p	pressure
P	periodic component of pressure variable
P_k	production of the turbulent kinetic energy
Re_H	Reynolds number based on H
Re_D	Reynolds number based on D
Re_p	Reynolds number based on particle dimension
S_{ij}	strain rate tensor
t	time
T	turbulent time scale
$\mathbf{U}$	time averaged velocity vector
$\mathbf{u}$	time fluctuation velocity vector
u_D	Darcian velocity
V	total volume of porous media
V_f	volume of fluid in porous media
$\overline{v^2}$	normal to the wall component of Reynolds stress
x_i	coordinate components

Greek Letters

β	overall pressure drop gradient
ε	dissipation rate of turbulent kinetic energy
φ	porosity
ν	kinematics viscosity
ν_t	turbulent viscosity
ρ	density

REFERENCES

1. Dybbs and Edwards, R.V. "A new look at porous media fluid mechanism - Darcy to turbulent", in *Fundamentals of Transport Phenomena in Porous Media (Book)*, J. Bear and V. Corapcioglu, M. Nijhoff, Eds., the Netherlands, pp. 199-254 (1984).

2. Missirlis, D., Yakinthos, K., Palikaras, A., Katheder, K. and Goulas, A. "Experimental and numerical investigation of the flow field through a heat exchanger for aero-engine applications", *Int. J. of Heat and Fluid Flow*, **26**, pp. 440-458 (2005).

3. Yang, Y.T. and Hwang, C.Z. "Calculation of turbulent flow and heat transfer in a porous-baffled channel", *Int. J. of Heat and Mass Transfer*, **46**, pp. 771-780 (2003).

4. Garcia, N., Lara, J.L. and Losada, I.J. "2-D numerical analysis of near-field flow at low-crested permeable breakwaters", *Coastal Engineering*, **51**, pp. 991-1020 (2004).

5. Karim, M.F. and Tingsanchalil, T. "A coupled numerical model for simulation of wave breaking and hydraulic performances of a composite seawall", *Ocean Engineering*, **33**, pp. 1-15 (2005).

6. Masuoka, T. and Takatsu, Y. "Turbulence model for flow through porous media", *Int. J. Heat Mass Transfer*, **39**, pp. 2803-2809 (1996).

7. Alvarez, G., Bournet, P.E. and Flick, D. "Two dimensional simulation of turbulent flow and transfer through stacked spheres", *Int. J. Heat Mass Transfer*, **46**, pp. 2459-2469 (2003).

8. Antohe, B.V. and Lage, J.L. "A general two-equation macroscopic turbulence model for incompressible flow in porous media", *Int. J. Heat Mass Transfer*, **40**, pp. 3013-3024 (1997).

9. Getachew, D., Minkowycz, W.J. and Lage, J.L. "A modified form of the $k-\varepsilon$ model for turbulent flows of an incompressible fluid in porous media", *Int. J. Heat Mass Transfer*, **43**, pp. 2909-2915 (2000).
10. Kuwahara, F., Kameyama, Y., Yamashita, S. and Nakayama, A. "Numerical modeling of turbulent flow in porous media using a spatially periodic array", *J. Porous Media*, **1**, pp. 47-55 (1998).
11. Nakayama, A. and Kuwahara, F. "A macroscopic turbulence model for flow in a porous medium", *ASME J. Fluids Eng.*, **121**, pp. 427-433 (1999).
12. Pedras, H.J. and Lemos, J.S. "Macroscopic turbulence modeling for incompressible flow through undeformable porous media", *Int. J. Heat Mass Transfer*, **44**, pp. 1081-1093 (2001).
13. Pedras, H.J. and Lemos, J.S. "On the mathematical description and simulation of turbulent flow in a porous medium formed by elliptic rods", *ASME J. Fluids Eng.*, **123**, pp. 941-947 (2001).
14. Kuwahara, F., Yamane, T. and Nakayama, A. "Large eddy simulation of turbulent flow in porous media", *Int. Com. in Heat and Mass Transfer*, **33**, pp. 411-418 (2006).
15. Durbin, P.A. "Near-wall turbulence closure modeling without damping functions", *Theoretical and Computational Fluid Dynamics*, Chap. 3, pp. 1-13 (1991).
16. Durbin, P.A. "On the $k-\varepsilon$ stagnation point anomaly", *Int. J. of Heat and Fluid Flow*, **17**, pp. 89-90 (1995).
17. Durbin, P. "Separated flow computations with the $k-\varepsilon-\overline{v^2}$ model", *AIAA Journal*, **33** pp. 659-664 (1995).
18. Behnia, M., Parneix, S. and Durbin, P.A. "Prediction of heat transfer in an axisymmetric turbulent jet impinging on a flat plate", *Int. J. Heat Mass Transfer*, **41**, pp. 1845-1855 (1998).
19. Lien, F.S. and Kalitzin, G. "Computations of transonic flow with the v^2-f turbulence model", *Int. J. of Heat and Fluid Flow*, **22**, pp. 53-61 (2001).
20. Sveningsson, A. and Davidson, L. "Assessment of realizability constraints in v^2-f turbulence models", *Int. J. of Heat and Fluid Flow*, **25**, pp. 785-794 (2004).
21. Davidson, L., Nielsen, P.V. and Sveningsson, A. "Modification of the v^2-f model for computing the flow in a 3D wall jet", in *4th Int. Symp. on Turbulence Heat and Mass Transfer*, Antalya, Turkey (2003).
22. Kelkar, K.M. and Patankar, S.V. "Numerical prediction of flow and heat transfer in a parallel plate channel with staggered fins", *J. of Heat Transfer*, **109**, pp. 25-29 (1987).
23. Hannani, S.K., Stanislas, M. and Dupont, P. "Incompressible Navier-Stokes computations with SUPG and GLS formulations - a comparison study", *Computer Methods in Applied Mechanics and Engineering*, **124**, pp. 153-170 (1995).
24. Hannani, S.K. and Stanislas, M. "Incompressible turbulent flow simulation using a Galerkin/least-squares formulation and a low Reynolds $k-\varepsilon$ model", *Comput. Methods Appl. Mech. Engineering*, **181**, pp. 107-116 (2000).
25. Hannani, S.K. and Stanislas, M. "Finite element simulation of turbulent Coutte-Poiseuille flows using a low Reynolds $k-\varepsilon$ model", *Int. J. Num. Methods in Fluids*, **30**, pp. 83-103 (1999).